Peer-reviewed version available at Sustainability 2019, 11, 5517; doi:10.3390/su11195517

Article

Landscape Changes and their Impacts on Land Surface Temperature in Tropical Hill Stations in South Asia: A Case Study of Nuwara Eliya, Sri Lanka

Manjula Ranagalage [1,2] *, Yuji Murayama [1], DMSLB Dissanayake [2,3,] *, and Matamyo Simwanda [4]

[1] Faculty of Life and Environmental Sciences, University of Tsukuba, 1-1-1, Tennodai, Tsukuba, Ibaraki 305-8572, Japan.
[2] Department of Environmental Management, Faculty of Social Sciences and Humanities, Rajarata University of Sri Lanka, Mihintale 50300, Sri Lanka.
[3] Graduate School of Life and Environmental Sciences, University of Tsukuba, 1-1-1, Tennodai, Tsukuba, Ibaraki 305-8572, Japan.
[4] Department of Plant and Environmental Sciences, School of Natural Resources, Copperbelt University, P.O. Box 21692, Kitwe 10101, Zambia.
* Correspondence: manjularanagalage@ssh.rjt.ac.lk or manjularanagalage@gmail.com (M.R.); dissanayakedmslb@gmail.com (D.D)

Abstract: Although urbanization has contributed to improving living conditions, it has had negative impacts on the natural environment in the urbanized areas. Urbanization has changed the urban landscape and resulted in increasing land surface temperature (LST). Thus, studies related to LST in various urban environments have become a popular research topic. However, few LST studies focusing on the mountain landscapes (i.e. hill stations) have been carried out. The primary objective of this study is to investigate changes in the landscape and their impacts on LST intensity (LSTI) in the tropical mountain city of Nuwara Eliya, Sri Lanka. The study utilized annual median temperatures extracted from Landsat data collected from 1996 to 2017 based on the Google Earth Engine (GEE) interface. The fractions of built-up (BL), forest (FL), and agricultural (AL) land were calculated using land use and cover maps based on the urban-rural zone (URZ) analysis. The urban-rural margin was demarcated based on the fraction of BL (<10%) and LSTI was measured using the mean LST difference in the urban-rural zone. In addition, the mixture of land use types was calculated using the AL/FL and BL/FL fraction ratios, and grid-based density analysis. The result shows that the BL in all URZ rapidly developed, while AL decreased during the period 1996 to 2017. There was minimal change in the forest area of the Nuwara Eliya owing to the government forest preservation policies. The fraction of the BL increased from 32.4% in 1996 to 58.7% in 2017 in the city center zone (URZ_1) resulting in increased mean LST by 4.7 °C. Furthermore, the increase of the BL/FL fraction ratio and the decrease of the AL/FL fraction ratio were positively correlated with the mean LST. Grid-based analysis showed an increasing positive relationship between mean LST and density of BL. This indicated that BL density has been a crucial element in increasing LST in the study area. The results of this study will be a useful indicator to introduce improved landscape and urban planning in the future to minimize the negative impact of LST on urban sustainability.

Keywords: land use and cover; land surface temperature, built-up land; agricultural land; gradient analysis; Nuwara Eliya; Sri Lanka

1. Introduction

In recent decades, population growth and economic development have directly affected the landscape transformation in developing countries [1]. Rapid changes in the landscape have resulted in the conversion of natural vegetation and agricultural land into built-up (impervious) land, such as

buildings, parking lots, roads, and other constructions [1–4]. This has caused several environmental problems at local, regional, and global scales [5], such as decreases in agricultural land [6]; habitat destruction [5,7,8]; air, soil, and water contamination [9,10]; increases in vector-borne diseases, such as malaria and dengue [11]; decreases in green space [12,13]; and increases Land Surface Temperature (LST) [14–16].

Increasing LST is an outcome of rapid urbanization and anthropogenic activities [17]. Built-up areas have been formed using several materials such as concrete, flooring, pebbles, stone, and gravel which decrease evapotranspiration, increase the sensitivity of the city and notably affect its local climate [15,18,19]. However, studying temperature changes based on the air temperature is challenging as there is a lack of meteorological stations, especially in developing countries [20]. Thus, satellite remote-sensing data provide vital information for observing the temperature pattern in urban areas [20]. Several studies have been conducted by using vast rage of remote sensing data, such as Modis data [21][22][23][24], SAR data [25], Nightlights data [26][27], Landsat data [16][28][29], Land Scan [30][31][32], and Fossil Fuel CO_2 Emission data [32][33] to understand the LST pattern. Many urban landscapes from small to large scales have been studied worldwide [15,34,35], including coastal cities [15,32,36,37], desert cities [19,38], and mountain cities [12,13]. Mountain cities are attractive for rich people as they have a cold climate and comfortable living conditions, which have resulted in rapid urban development [13]. Thus, studies related to the different mountain landscape are vital for understanding the changing pattern of LST to introduce mitigation measures for comfortable living conditions.

A large number of studies have used two or more satellite images in a different period to analyze the LST pattern due to the unavailability of the cloud-free images. However, the difference in the acquisition time might have influenced to LST pattern due to the influence of various environmental factors such as wind speed, surface moisture, humidity, and Sun's radiation [31][4]. The use of more satellite images captured in multiple time point can potentially provide more specific information to understand the changing pattern of LST [4]. Still, it is not easy to analyze extensive earth observation data set due to spatial and temporal resolution [39][40]. Thus, big data analysis platforms can be used as an alternative for conducting accurate result [39]. Google Earth Engine (GEE) provides potential to process a large number of satellite images, and researchers can easily access to free public data archives more than thirty years of historical data [39]. Hence, we have used GEE to extract the annual median LST for three-time points such as 1996, 2006, and 2017 based on the several images captured during the selected years. We hypothesized that the use of many images captured in multiple time points provides a clear picture of the LST pattern of the study area.

The spatial distribution of the LST intensity (LSTI) provides essential environmental information for understanding the temperature pattern in detail. Two methods can be used to study LSTI, such as (1) categorization of land use and cover as the local climate zone and following the cross cover comparison method used to calculate the LSTI [12,13,41–43], and (2) determining the difference in the mean LST between urban and rural zones based on the urban-rural gradient analysis. The mean LST, a fraction of built-up land (BL), and green spaces have been used in previous studies [12,13]. The urban-rural demarcation is essential for determining the temperature difference. In this study, we calculated the gradient zone as the <10% fraction of BL from the city center [12,13]. The AL was considered as a part of green spaces in most of the previous studies [12,13]. However, we used a separate fraction of AL to understand the LSTI by considering the spatial distribution in Nuwara Eliya.

Mountain cities in Asia have been developing since the colonization period of the 19th and 20th centuries [44,45]. The cool climate and natural landscape became the most prominent factors driving the development of mountain cities. During the colonial period, cool climates were preferred as they allowed the Colonials to maintain their "western lifestyle." However, mountain cities were also selected as the population could avoid wasting illnesses, episodic pestilence, sunstroke, and depression [44,46]. Most mountain cities underwent rapid urbanization after World War II, and the rapid development of the urban landscape and population growth are becoming vital for understanding the urban development process in Asian hill stations [44]. Thus, most of the negative

by-products of urbanization can be observed in the mountain cities, and similar patterns can be seen in the mountain cities of Sri Lanka [12].

Nuwara Eliya is a historical city that developed during the British colonial period, reflected in the city's architecture [47]. The British people preferred a cold climate, and Nuwara Eliya was referred to as "Little England" [47]. They used Nuwara Eliya as a meeting place for wealthy British families [48]. Currently, several recreational sites, such as Lake Gregory, golf links, race courses, and a large number of clubs, remain in Nuwara Eliya [48]. After gaining independence in 1948, Nuwara Eliya became renowned worldwide as a tourist destination in Sri Lanka, and thousands of tourists from Sri Lanka and overseas visited this area to enjoy the cool climate and natural beauty [47]. This has resulted in the occurrence of several environmental problems associated with urbanization. Thus, we hypothesize that the rapid changes in the urban landscape caused the LST pattern in the study area. Most previous studies related to LST focused on the Colombo City [3,4,36] and Kandy [12][49] in Sri Lanka. This study examines the changes in the urban landscape and their impact on the spatial changes of LST to introduce proper landscape and urban planning in Nuwara Eliya. Thus, the objectives of this study are to (1) monitor the urban landscape changes and their impact on the LST intensity over the past 21 years (1996 -2017) based on the urban-rural gradient analysis; (2) identify relationships between mean LST and the AL/FL and BL/FL fraction ratio; and (3) study the relationship between mean LST and density of BL, FL, and AL based on the grid-based analysis method. The result of this study can be used to enhance capacity and knowledge to minimize the possible negative impacts of rapid urbanization in the study area.

2. Materials and Methods

2.1. Study area: Nuwara Eliya, Sri Lanka

Nuwara Eliya is located in the central province of Sri Lanka and resides at latitudes of 6°54'21.94" to 7°2'28.53" N and longitudes of 80°50'5.89" to 80°41'57.23" E (Figure 1). The study area includes the landscape within a 7.5 km2 radius of the center of Nuwara Eliya. Nuwara Eliya is surrounded by one of the tallest mountains (~ 2,524 m high) in the study area known as Pidurutalagala. The average elevation of Nuwara Eliya is about 1,800 m. Monthly rainfall in Nuwara Eliya ranges from approximately 71.5 to 226.8 m, with an annual average of 1,905 mm. The lowest average monthly rainfall is recorded in January, February, and March, resulting in a relatively dry period. According to the Meteorology Department of Sri Lanka, the daily mean temperature is about 15.9 °C, with average minimum and maximum temperatures of 11.6 and 20.2 °C, respectively. Nuwara Eliya is the most popular site among local and foreign tourists due to the cold climate that persists throughout the year. In terms of the urban development pattern, Nuwara Eliya exhibits a single core concept.

Preprints (www.preprints.org) | NOT PEER-REVIEWED | Posted: 26 August 2019 doi:10.20944/preprints201908.0262.v1

Peer-reviewed version available at Sustainability 2019, 11, 5517; doi:10.3390/su11195517

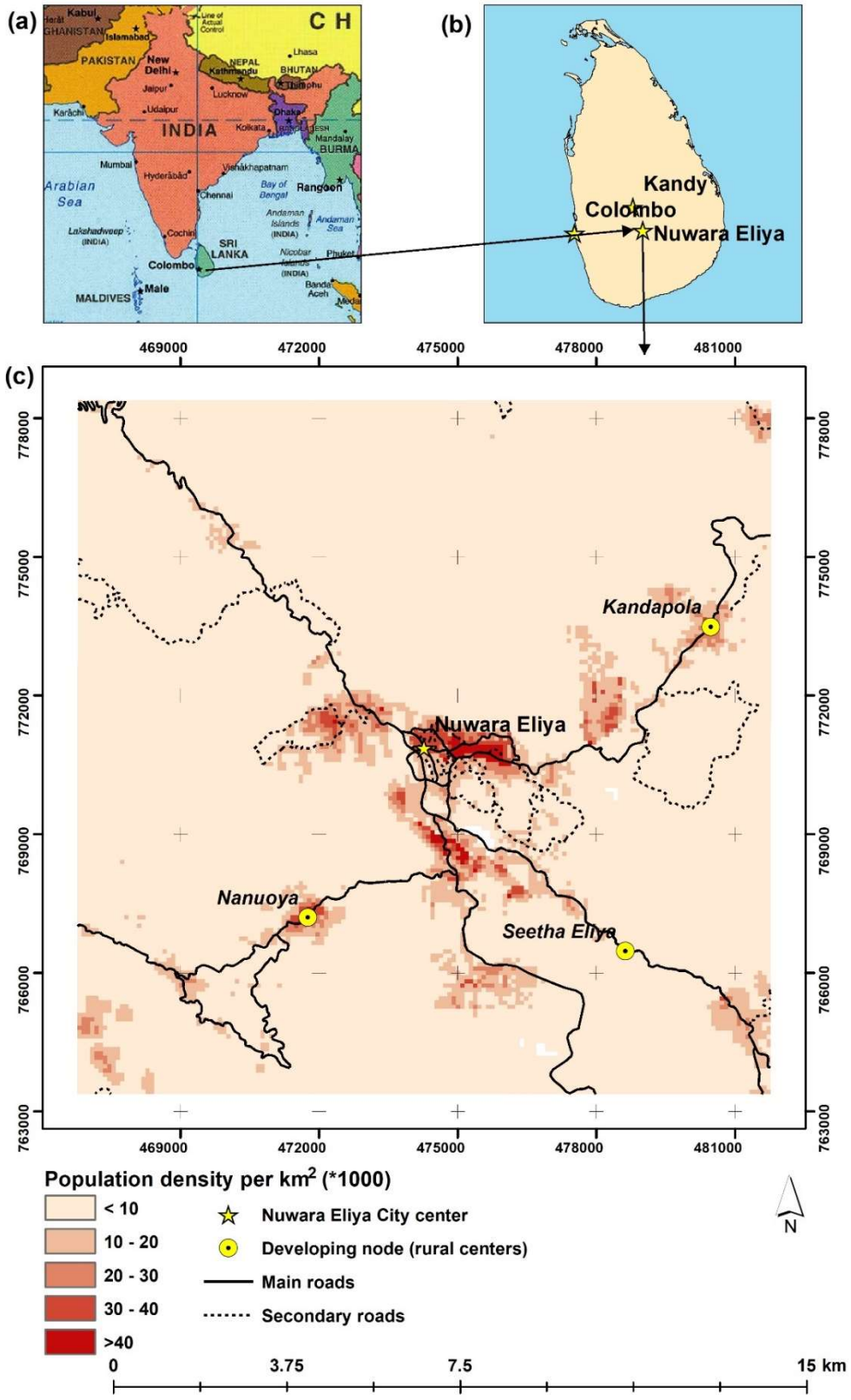

Figure 1. Study area: **(a)** Map of South Asia (http://www.maps-world.net); (**b**) Location of Nuwara Eliya; and (**c**) Population density of Nuwara Eliya (100 × 100 m).

2.2. Overall workflow

Figure 2 shows the overall workflow of the study to achieve the objectives described above. The study workflow included five major steps: (i) extraction of median upper-atmosphere brightness

temperature from the thermal bands of the Landsat images (Figure 2a); (ii) retrieval of LST (Figure 2b); (iii) LULC classification into five classes, forest land (FL), built-up (BL), agriculture land (AL), other land, and water using machine learning algorithms based on supervised classification (Figure 2c); (iv) urban-rural gradient, statistical and intensity analysis based on the BL, FL and AL fractions, AL/FL and BL/FL ratios and mean LST and finally (v) grid analysis based on the mean LST and the density of BL, FL, and AL.

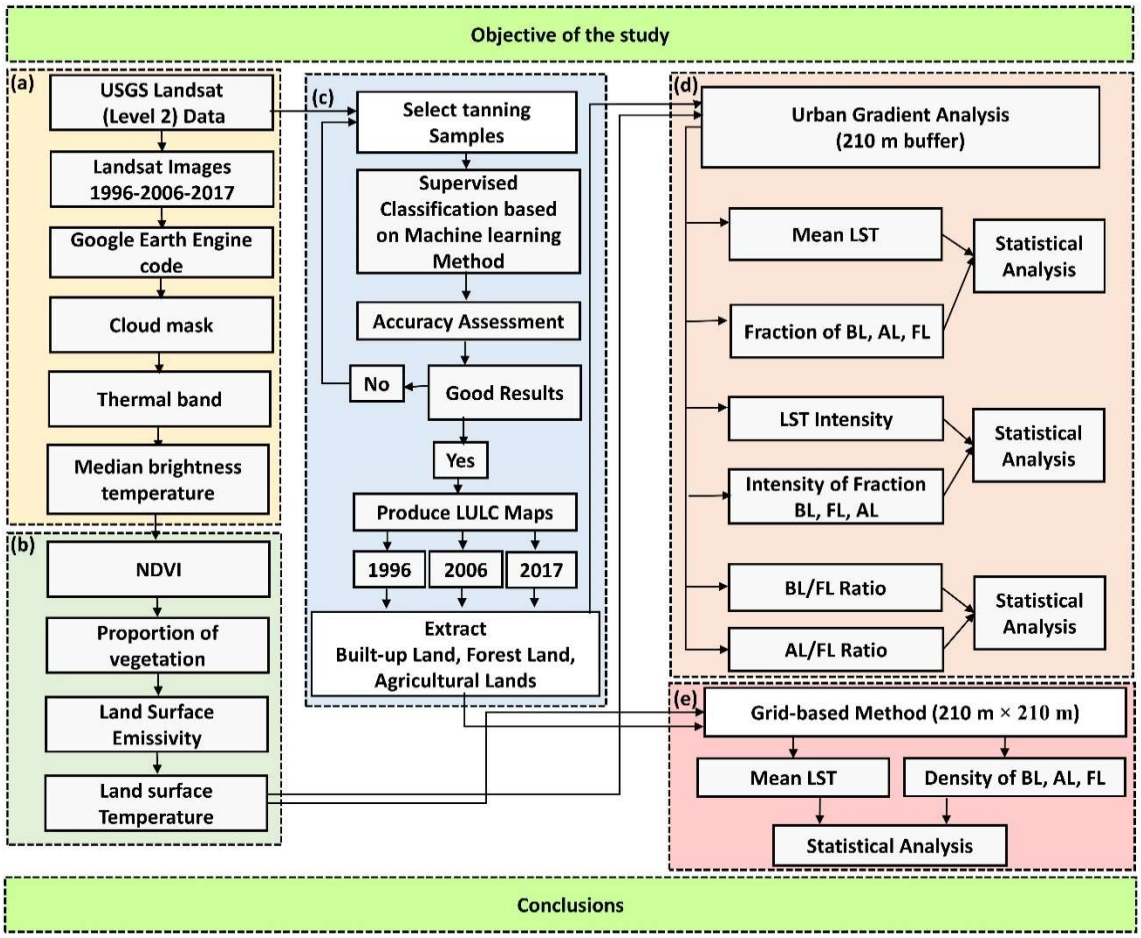

Figure 2. Workflow of the study. Note BL, FL and AL refers to built-up land, forest land, and agriculture land, respectively

2.3. Satellite data preparation using Google Earth Engine (GEE)

The study employed the GEE to calculate at-satellite brightness temperature using atmospherically corrected pre-processed datasets (Level 2) [50]. In this process, several steps were performed as follows. First, the study area was defined and imported as "Assets" in GEE, and thereafter used as the primary geometry throughout the process. Masking was then conducted due to cloud disturbance in the available Landsat imageries. The cloud disturbance could be attributed to Nuwara Eliya being located in a tropical area. Afterwards, the Image Collection tool in GEE was used to prepare the imageries for the study including 15 images for 1996 (Landsat 5), 17 images for 2006 (Landsat 5), and 20 images for 2017 (Landsat 8) (Table A1). The Figure 3 shows the graphical illustration of creating image collection and the code used to generate median pixel values of imageries is provided in Annex A2 and A3.

Peer-reviewed version available at Sustainability 2019, 11, 5517; doi:10.3390/su11195517

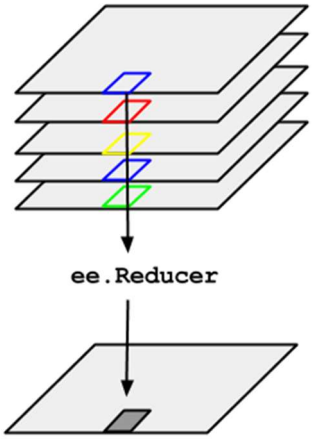

Figure 3. Graphical illustration of image collection

(Source: https://developers.google.com/earth-engine/reducers_image_collection)

Finally, median pixel values of each image were selected and three data sets were prepared in each year [51] (Figure2). To do this, all thermal bands in the Landsat imageries were used to generate annual median temperatures based on the upper-atmosphere brightness temperature for the thermal bands (in Kelvin). On the other hand, the multispectral bands were used to calculate the best median pixel of the imageries for the study area. The extracted thermal band (band 6 for Landsat 5 and band 10 for Landsat 8) were used to calculate the LST (section 2.4). We hypothesized that the use more imageries produces clearer output images to understand the LST patterns in the study area. Past studies have shown the aptness of this method to generate LST in different areas [39][40]. All extracted images were georectified using the WGS84/UTM 44N projection system before further processing.

2.4. LST calculation

The extracted median at-satellite brightness temperature in section 2.3, was scaled using the land surface emissivity derived from Equation. (1) [52].

$$\varepsilon = \{mPV + n\} \quad (1)$$

where m = (ε − ε) − (1 − εσ) Fεv and n = εs + (1 − εs) Fεv, where εs and εv are the soil emissivity and vegetation emissivity, respectively. In this study, we used the result of [52] for m = 0.004 and n = 0.986. The proportion of vegetation (P_v) was calculated using the normalized difference vegetation index (NDVI) based on Equation. (2)[53].

$$NDVI = \frac{\rho_{NIR} - \rho_{Red}}{\rho_{NIR} + \rho_{Red}} \quad (2)$$

where ρ_{NIR} refers to the surface reflectance values of Bands 4 (Landsat-5) and 5 (Landsat-8); and ρ_{Red} refers to the surface reflectance values of Bands 3 (Landsat-5), and 4 (Landsat-8 OLI).

P_v was extracted using Equation. (3)

$$P_v = ((NDVI - NDVI_{min})/(NDVI_{max} - NDVI_{min}))^2 \quad (3)$$

where, P_v is the proportion of vegetation, NDVI is original NDVI values calculated using Eq. (2), and $NDVI_{min}$ and $NDVI_{max}$ are the minimum and maximum values of the NDVI dataset, respectively.

The emissivity corrected images were used to extract LST using Equation. (4) [3,29].

$$LST = T_b / 1 + (\lambda \times T_b / \rho) \ln \varepsilon \quad (4)$$

where T_b is the at-satellite brightness temperature in degrees Kelvin; λ is the central band wavelength of emitted radiance (11.5 μm for Band 6 [29] and 10.8 μm for Band 10 [12]; ρ is $h \times c/\sigma$ (1.438×10^{-2} m K), with σ as the Boltzmann constant (1.38×10^{-23} J/K), h as Planck's constant (6.626×10^{-34} J *s), and c as the velocity of light (2.998×10^{8} m/s); and ε is the land-surface emissivity estimated using the NDVI method [52]. The calculated LST value (Kelvin) was then converted to °C.

2.5. Land Use/Land Cover (LULC) Mapping

Machine learning methods such as the support vector machine, K-nearest neighbor, random forest, and neural networks, have been widely used to classify LULC [12][13]. Among these methods, the support vector machine (SVM) has provided higher overall accuracy [54][55][56][57]. Thus, in this study, we used the SVM algorithm to conduct LULC mapping. The classification scheme used in the study included five LULC categories including Built-up land (BL), Forest land (FL), Agricultural land (AL), Other lands and Water. The Other lands category comprised a combination of grasslands and bare lands.

We produced three LULC maps containing the five LULC categories (BL, FL, AL, other land and water) for the years 1996, 2006, and 2017 with overall accuracies of 85%, 93%, and 92%, respectively (see Tables A4, A5, and A6). The accuracy was assessed by using 500 reference points generated by a stratified random sampling method [13] for all the LULC categories. Google Earth imageries were used to assess the accuracy of the classified LULC maps for 2006 and 2017. The accuracy assessment for the 1996 LULC map was conducted with the aid of the available topographic maps and different band combinations of Landsat imageries.

2.6. LST intensity (LSTI) measurement

The LSTI was calculated based on the urban-rural gradient analysis approach involving the creation of concentric rings or buffer zones around the city center with standard distance intervals extending to the rural areas [12,13,41]. Urban-rural gradient analysis has been conducted to identify the spatial and temporal variations in environmental variables in many previous environmental studies [12,13,15,19,58][59]. In this study, thirty five 210-meter buffer zones (hereinafter referred to as urban-rural zones (URZs)) were created for the study area. The mean LST of each URZ was then extracted using zonal statistics. The fractions of BL, FL, and AL were determined by calculating their respective proportions in each URZ. Of note is that previous studies combined AL and FL into one LULC category, defined as green space [12,13,15]. However, AL has been one of the key drivers of LULC changes in the study area. Therefore, AL in Nuwara Eliya and its surroundings was considered separately.

The magnitude of the LSTI along the urban-rural gradient ($LSTI_{U\text{-}R}$) was determined based on the Δ mean LST, Δ fraction of BL, Δ fraction of FL, and Δ fraction of AL following methodology proposed by Estoque and Murayama [13]. To calculate $LSTI_{U\text{-}R}$, we first determined the Δ mean LST by finding the difference between the mean LST in the URZ with the highest fractions of BL, FL and AL (defined as URZ_1) and other URZ_s (i.e. $URZ_1 - URZ_{2 \ldots 35}$). We then applied the same method to determine the Δ fraction of BL, Δ fraction of FL, and Δ fraction of AL along the urban-rural gradient. We used the same threshold for delineating the urban and rural zones as [12,13] i.e., from the city center, all URZs with >10% fraction of BL were considered as urban and those beyond the first URZ with <10% fraction of BL were considered as rural.

2.7. AL/FL and BL/FL fraction ratios and their intensities

The AL/FL and BL/FL fraction ratios were calculated using the URZs created in 2.6. Ranagalage et al., 2018 [12] proposed the green space (GS)/impervious surface (IS) fraction ratio and its intensity, and we followed their methodology to extract AL/FL and BL/FL in each URZ using Equations. 5 and 6, respectively.

$$\text{AL/FL fraction ratio} = \frac{\text{ALz}}{\text{FLz}} \quad (5)$$

$$\text{BL/FL fraction ratio} = \frac{\text{BLz}}{\text{FLz}} \quad (6)$$

2.8. Grid-based analysis

The grid-based method was used to analyze the spatial distribution of the density of BL, FL, AL, and mean LST in 1996, 2006, and 2017. In this analysis, we used 210m × 210 m grids (7 × 7 pixels) to demarcate the relationship between BL, FL, AL density with mean LST. The 210 × 210 m grid size was used in previous studies and achieved high correlation with mean LST [15][38][43][60]. After the creation of the set of grids, the mean LST and the densities of BL, FL, and AL in each grid were calculated. The scatter plots were created, and linear regression analysis was performed to identify the relationships between mean LST and density of BL, FL, and AL.

3. Results

3.1. Landscape Changes and LST Distribution of Nuwara Eliya

The results revealed that Nuwara Eliya experienced rapid urbanization in the last 21 years. The built-up area increased from 289.9ha to 2,080.4 ha from 1996 to 2017, with an annual growth rate of 85.3 ha per year (Figure 4 and Tables 1 and 2). The forest area has not changed significantly due to the implementation of forest reserves [61]. Rapid changes in the built-up land have negatively affected the agricultural sector. The area of agricultural land decreased from 8,503.2 ha to 6,583.9 ha from 1996 to 2017 (Table 1). The rapid changes in the landscape have also directly affected the spatial changes of LST in the study area.

Table 1. Details of the LULC changes in Nuwara Eliya (1996, 2006, and 2017)

Land Use/Cover	1996		2006		2017	
	Area (ha)	%	Area (ha)	%	Area (ha)	%
Built-up	289.9	1.3	785.5	3.5	2080.4	9.3
Forest	13,076.7	58.2	13,502.1	60.1	13,234.3	58.9
Agricultural Land	8,503.2	37.9	8,085.5	36.0	6,583.9	29.3
Other Land	511.8	2.3	6.0	0.0	481.8	2.1
Water	73.4	0.3	75.9	0.3	74.6	0.3
Total	22,455.0	100.0	22,455.0	100.0	22,455.0	100.0

Peer-reviewed version available at Sustainability 2019, 11, 5517; doi:10.3390/su11195517

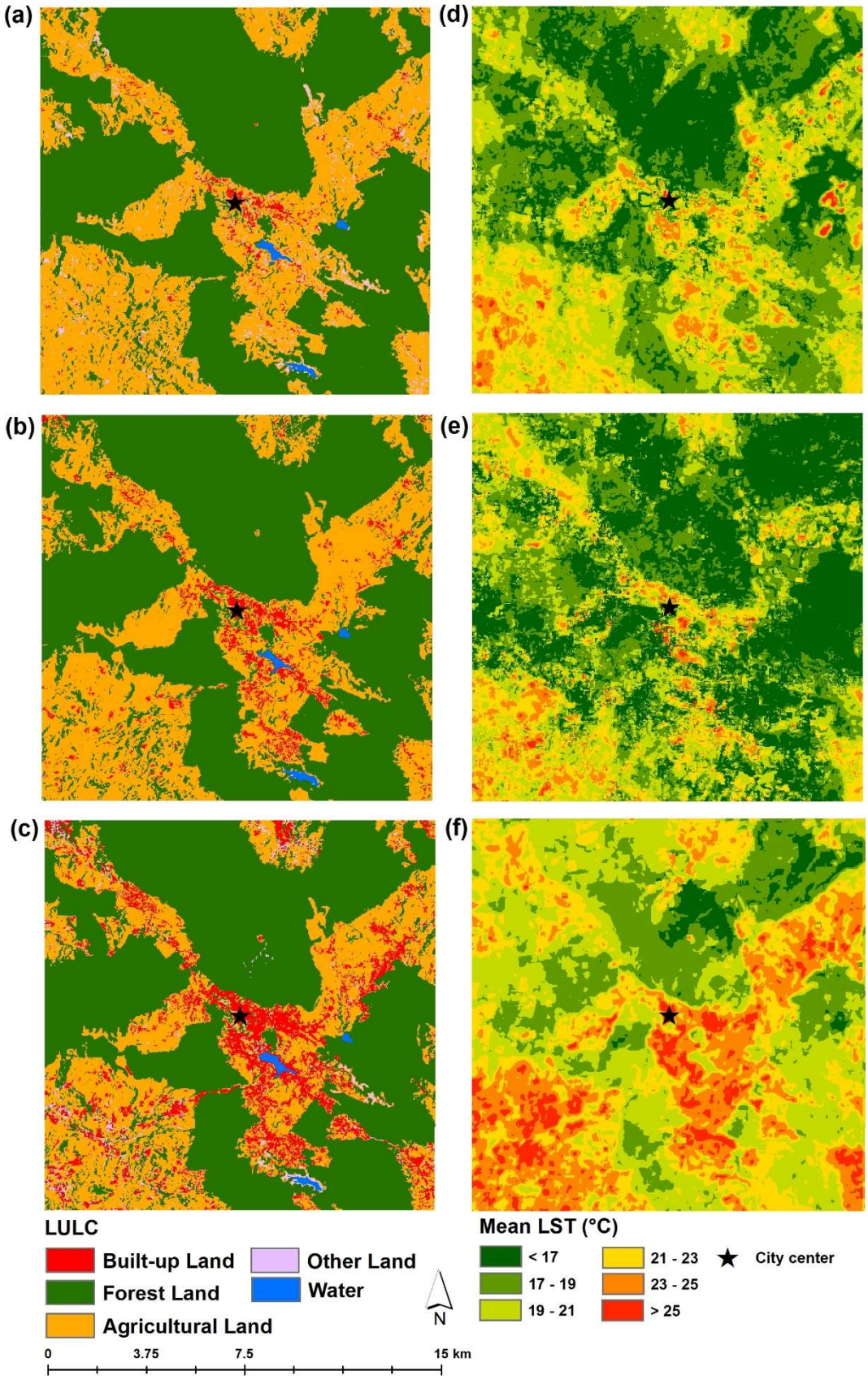

Figure. 4. Land use/cover maps and LST values in Nuwara Eliya: land use/cover in (**a**) 1996, (**b**) 2006, and (**c**) 2017; and LST in (**d**) 1996, (**e**) 2006, and (**f**) 2017.

Table 2. LULC changes during 1996-2006, 2006-2017, and 1996-2017.

Land Use/Cover	1996-2006		2006-2017		1996-2017	
	Land use/cover changes (ha)	Annual growth rate (ha per year)	Land use/cover changes (ha)	Annual growth rate (ha per year)	Land use/cover changes (ha)	Annual growth rate (ha per year)
Built-up	495.6	49.6	1,294.9	117.7	1,790.6	85.3
Forest	425.3	42.5	-267.8	-24.3	157.6	7.5
Agricultural Land	-417.7	-41.8	-1,501.7	-136.5	-1,919.3	-91.4
Other Land	-505.8	-50.6	475.7	43.2	-30.1	-1.4
Water	2.5	0.3	-1.3	-0.1	1.3	0.1

Figure 4 (d, e, f) shows the spatial distribution of LST in Nuwara Eliya for the years 1996, 2006, and 2017, respectively. In 1996, LST ranged between 9.1 and 29.2 °C, with a mean value of 18.9 °C. In 2006, LST ranged between 5.9 and 30.2 °C, with a mean value of 17.9 °C. In 2017, LST ranged between 14.3 and 31.0 °C, with a mean value of 21.0 °C. Therefore, the mean LST exhibited an increasing trend from 1996 to 2017. The mean LST increased by 2.1 °C during the past 21 years.

3.2. Magnitude and Trend of LSTI

3.2. 1. $LSTI_{U-R}$ along the Urban-Rural Gradient

Figure 5 (a, b, c) shows the spatial pattern of mean LST, and the fractions of BL, FL, and AL along the urban-rural gradient. The highest mean LST value was recorded in the URZ_1 zone near the city center. In 1996, the mean LST of URZ_1 was 19.8 °C, which decreased to 18.9 °C in 2006 and increased to 24.4 °C in 2017. Conversely, the mean LST of all other URZs increased from 1996 to 2017. The results revealed that the mean LST of all other URZs was 18.9 °C and 21.2°C in 1996 and 2017, respectively. The results further revealed that the lowest temperatures were recorded in URZ_{12} in 1996, URZ_{10} in 2006, and URZ_{19} in 2017 (Figure 5).

The fraction of BL increased rapidly between 1996 and 2017. In URZ_1, the fraction of BL increased by 32.4%, 48.7%, and 58.7%, in 1996, 2006, and 2017, respectively. The fraction of FL did not significantly change during the last 21 years. However, rapid changes in AL occurred in all URZ throughout the study temporal extent. The lowest fraction of AL was always recorded in URZ_1 and exhibited a decreasing pattern. The AL fraction in URZ_1 was 43.6% in 1996, 29.6% in 2006, and 15.8% in 2017.

Figure 5b shows the results of the statistical analysis of mean LST with the fractions of BL, FL, and AL. The mean LST had a significant strong positive correlation ($p < 0.001$) with the fraction of BL at all the three time-points. The fraction of FL exhibited a significantly strong negative correlation ($p < 0.001$) with mean LST. On the other hand, mean LST exhibited a dissimilar relationship with the fraction of AL in 1996, 2006, and 2017. In 1996, the mean LST had a significant positive correlation ($p < 0.001$) with the fraction of AL. In 2006, the mean LST and fraction of AL had a weak relationship ($p < 0.5$), and, in 2017, the mean LST had a significant negative correlation with the fraction of AL ($p < 0.1$).

Peer-reviewed version available at Sustainability 2019, 11, 5517; doi:10.3390/su11195517

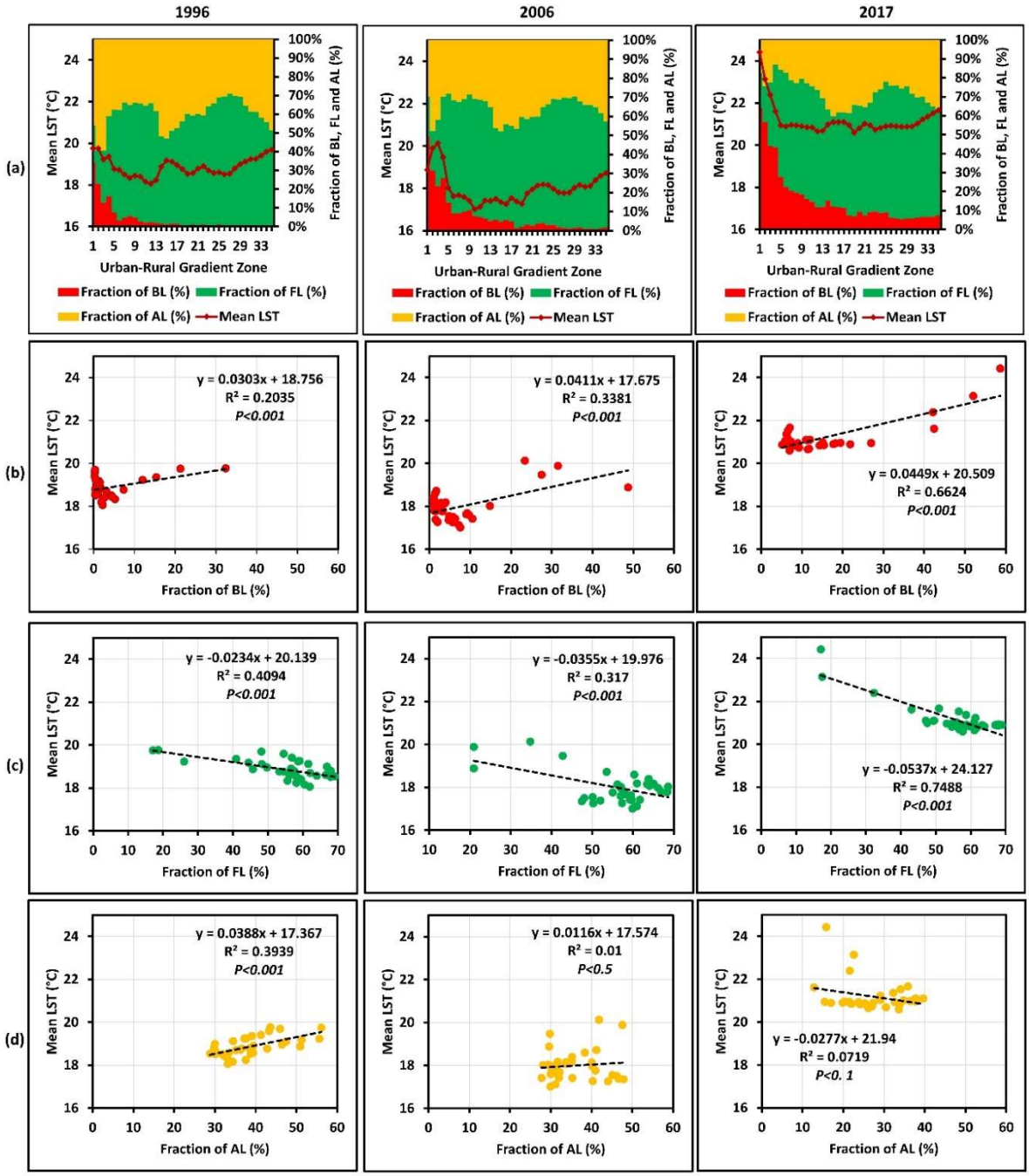

Figure. 5. (**a**) Spatial distribution of mean LST, and the fractions of BL, FL, and AL along the urban-rural gradient; and scatter plots of the mean LST and fractions of (**b**) BL, (**c**) FL, and (**d**) AL.

3.2. 2. The magnitude of LSTI$_{U-R}$ along the Urban-Rural Gradient

The magnitudes of the mean LST and fractions of BL, FL, and AL were calculated based on URZ$_1$ as described in section 2.6 above. The Δ mean LST in URZ$_{13}$ showed a considerable decrease in 1996 and 2006. However, the decrease shifted to URZ$_{20}$ in 2017 (Figure 6a). The Δ fractions of BL, FL, and AL also showed a similar pattern. The statistical analysis revealed that the Δ mean LST had a significant positive relationship with the Δ fraction of BL, and a strong negative relationship with the Δ fraction of FL. The Δ mean LST exhibited a significant positive relationship in 1996 ($p < 0.001$) and in 2006 ($p < 0.5$) with the Δ fraction of AL. However, the relationship changed in 2017 showing a weak negative correlation ($p < 0.5$) with the Δ fraction of AL.

Peer-reviewed version available at Sustainability 2019, 11, 5517; doi:10.3390/su11195517

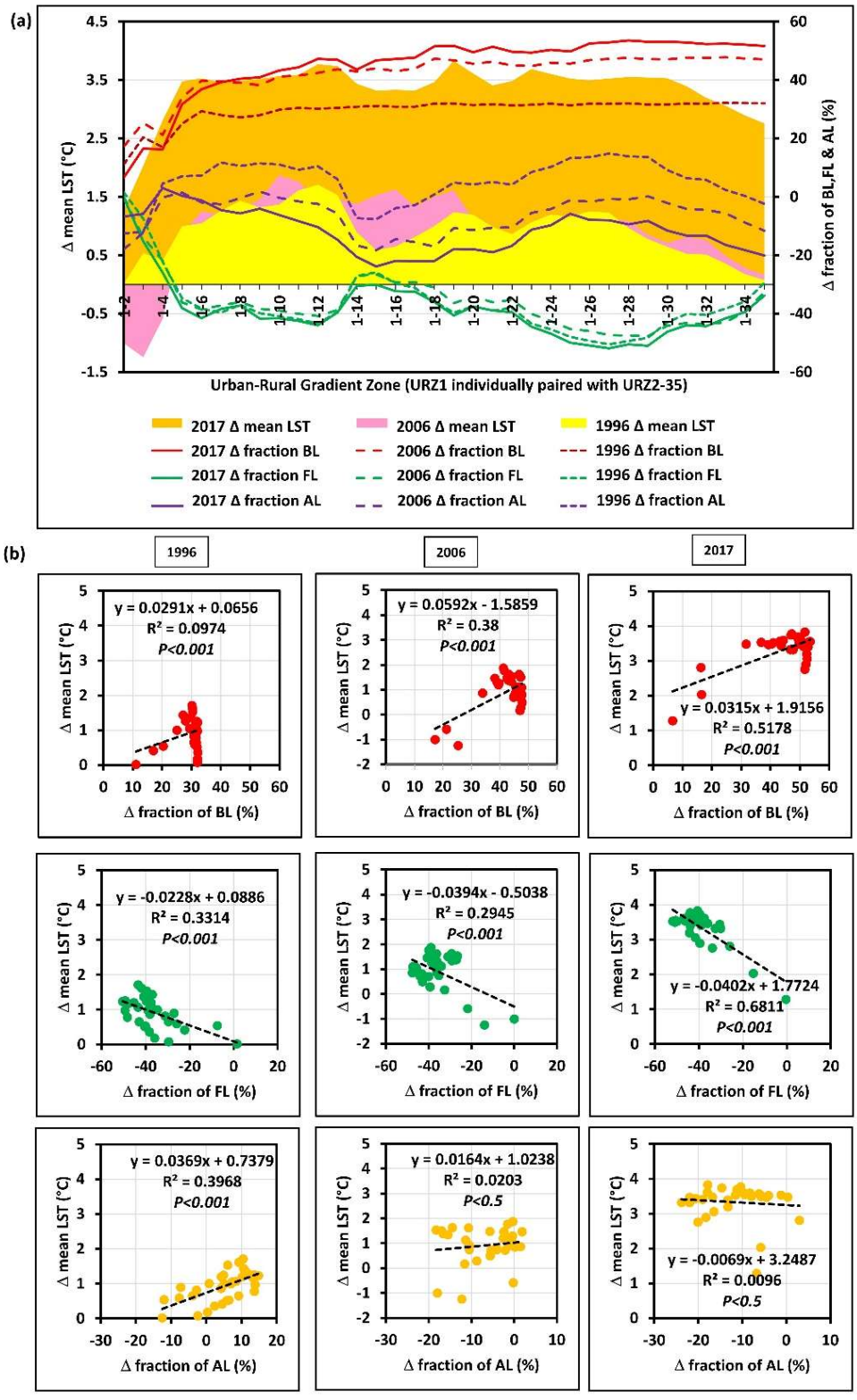

Figure. 6. (**a**) Magnitudes of the trends of $LSTI_{U-R}$ (°C), and fractions of BL, FL, and AL along the URZ; and (**b**) scatter plots and statistical relationships between the magnitude of mean LST and fractions of BL, FL, and AL in Nuwara Eliya during 1996, 2006, and 2017.

Peer-reviewed version available at Sustainability 2019, 11, 5517; doi:10.3390/su11195517

306 *3.3. AL/FL and BL/FL Ratios Along the Urban-rural Gradient*

307 An annual decrease in AL of 91.6 ha was observed from 1996 to 2017 (Table 2). FL was stable
308 due to the protection measures implemented by the Forest Department of Sri Lanka (Table 1). Figure
309 7a shows the spatial distribution of the mean LST and AL/FL fraction ratio. A rapid decreasing trend
310 in the AL/FL fraction ratio was observed from 1996 to 2017. The AL/FL fraction ratio decreased in all
311 zones from URZ_1 to URZ_{35} with average values of 0.84, 0.7, and 0.53 in 1996, 2006, and 2017,
312 respectively. The mean LST values had a significant ($p<0.001$) positive relationship with the AL/FL
313 fraction ratio. Figure 7 (c) shows the statistical relationship between the Δ mean LST and Δ AL/FL
314 fraction ratio along the urban-rural gradient, and the result shows a significant positive relationship
315 in all the three time-points in this study.

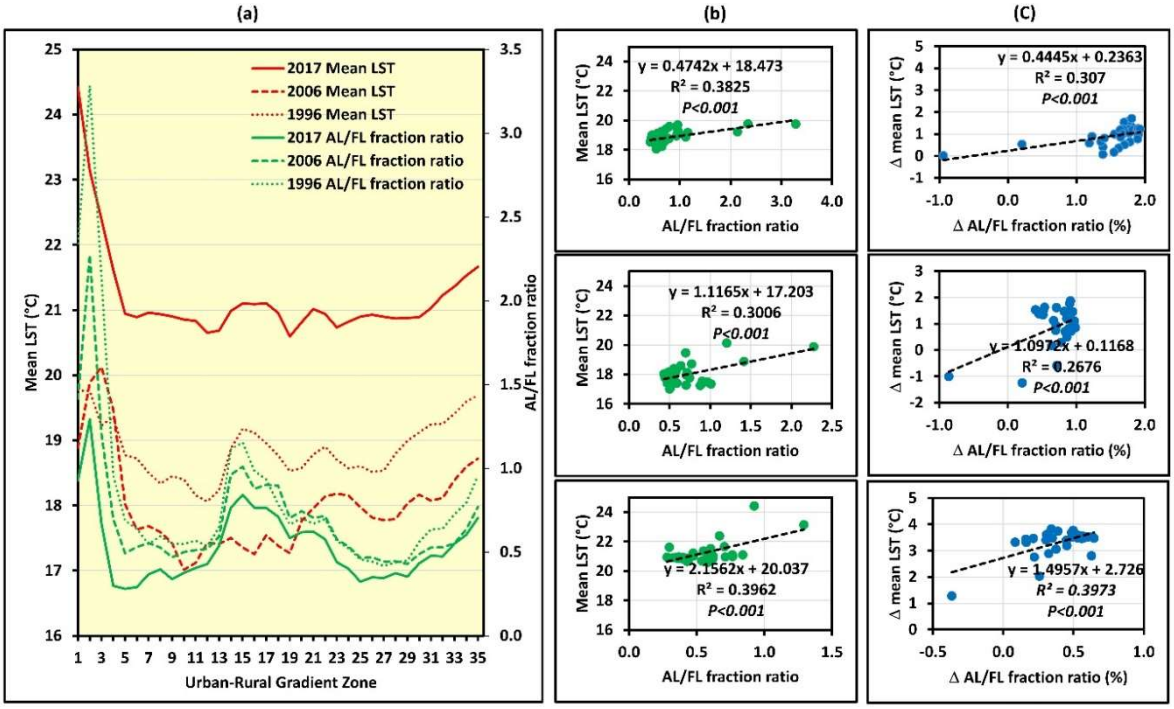

316

317 **Figure. 7.** (**a**) Spatial distribution of the mean LST, AL/FL fraction ratio; (**b**) scatter plots of the mean LST and
318 AL/FL fraction ratio; and (c) Δ mean LST (°C) and Δ AL/FL fraction ratio in Nuwara Eliya during 1996, 2006,
319 and 2017.

320 Figure 8a shows the spatial distribution of the mean LST and BL/FL fraction ratios. The BL/FL
321 ratio increased from 1996 to 2017 with average values of 0.13, 0.22, and 0.42 in 1996, 2006, and 2017,
322 respectively. The mean LST exhibited a significant ($p<0.001$) positive relationship with the BL/FL
323 fraction ratio (Figure 8b). The relationship between the Δ mean LST and Δ BL/FL fraction ratio is
324 presented in Figure 8c. The results revealed that there was a significant strong positive relationship
325 between the Δ mean LST and Δ BL/FL fraction ratio in all the three time-points.

326

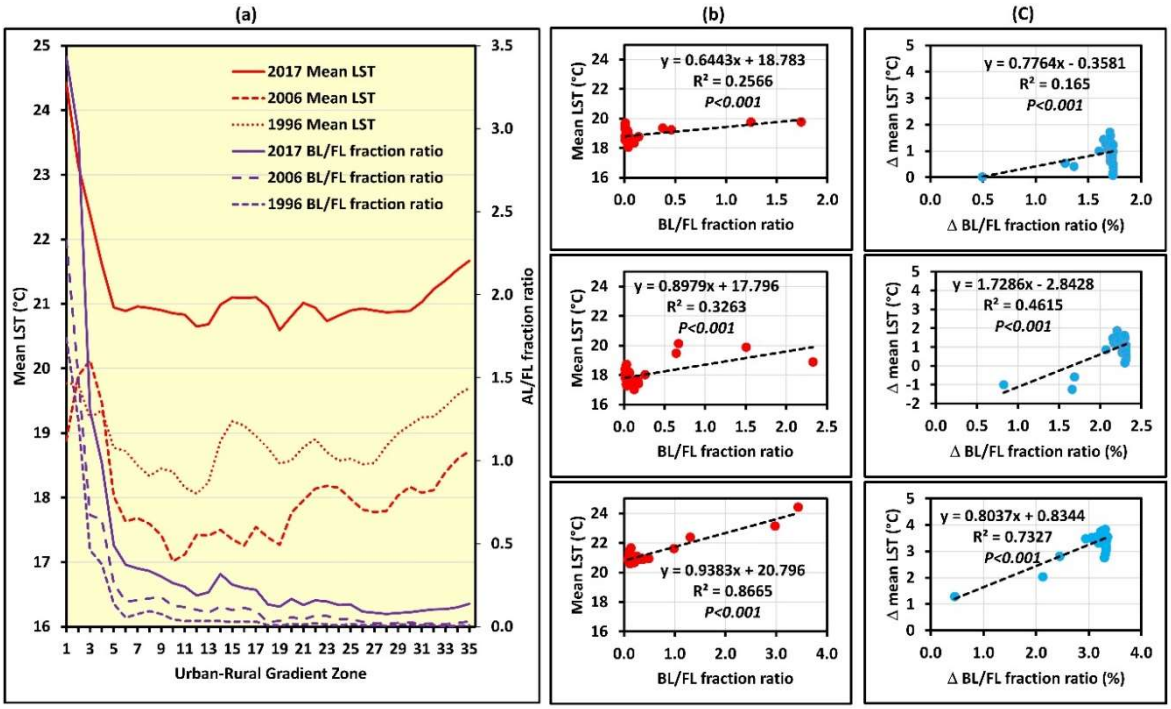

Figure. 8. (**a**) Spatial distribution of the mean LST and BL/FL fraction ratio; (**b**) scatter plots of the mean LST and BL/FL fraction ratio; and (c) Δ mean LST (°C) and Δ BL/FL fraction ratio in Nuwara Eliya in 1996, 2006, and 2017.

3.4. The density of BL, FL, and AL vs. mean LST

Figure 9a shows the spatial distribution of mean LST and the density of BL, FL, and AL in 1996, 2006, and 2017. High temperatures were observed around the city center and the northwestern and southwestern parts of the study area. The BL density was also high around the city center area in 1996 and it spread towards the south, southwestern and southeastern direction of the Nuwara Eliya area in 2006 and 2017. The FL density had an opposite pattern showing low FL densities around all areas of high BL densities in all the three time points. However, AL density showed a decreasing trend, especially in the city center area and southwestern direction of the study area.

Fig 9b shows the relationship between the densities of BL, FL, AL, and mean LST based on the grid-based analysis. The results show that mean LST was statistically significant ($p < 0.001$) with the densities of BL, FL, and AL in all the three time points. There was an increasing trend of a positive correlation between BL density and mean LST from 1996 to 2017. The correlation between mean LST and the density of FL showed a significant negative relationship throughout the study period. On the other hand, there was a decreasing trend of a positive correlation between AL density and mean LST from 1996 to 2017.

Peer-reviewed version available at Sustainability 2019, 11, 5517; doi:10.3390/su11195517

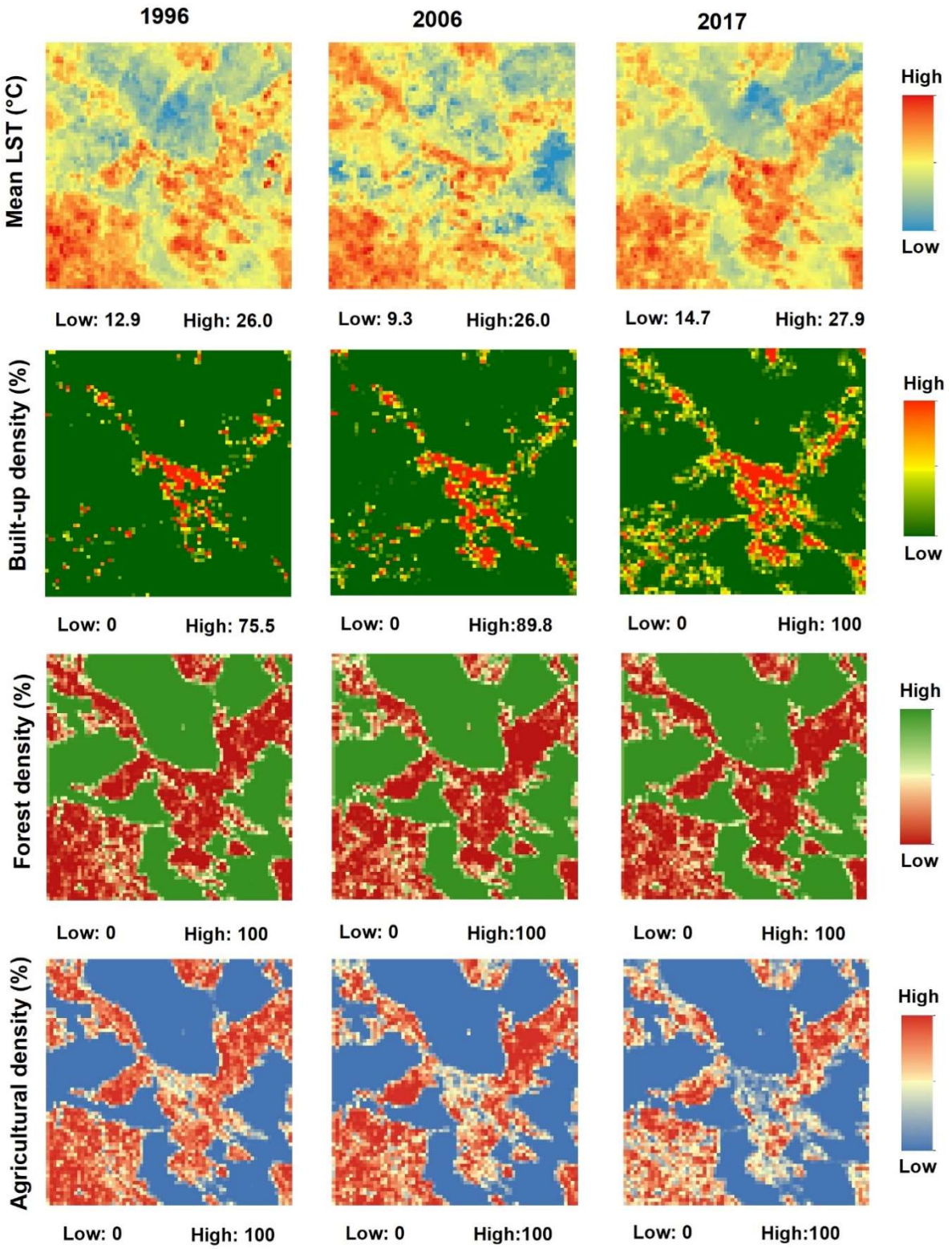

Figure. 9a. Graphical view of the 210 × 210 m polygon grid showing maps of mean LST, Built-up density, Forest density, and Agricultural density.

Peer-reviewed version available at Sustainability 2019, 11, 5517; doi:10.3390/su11195517

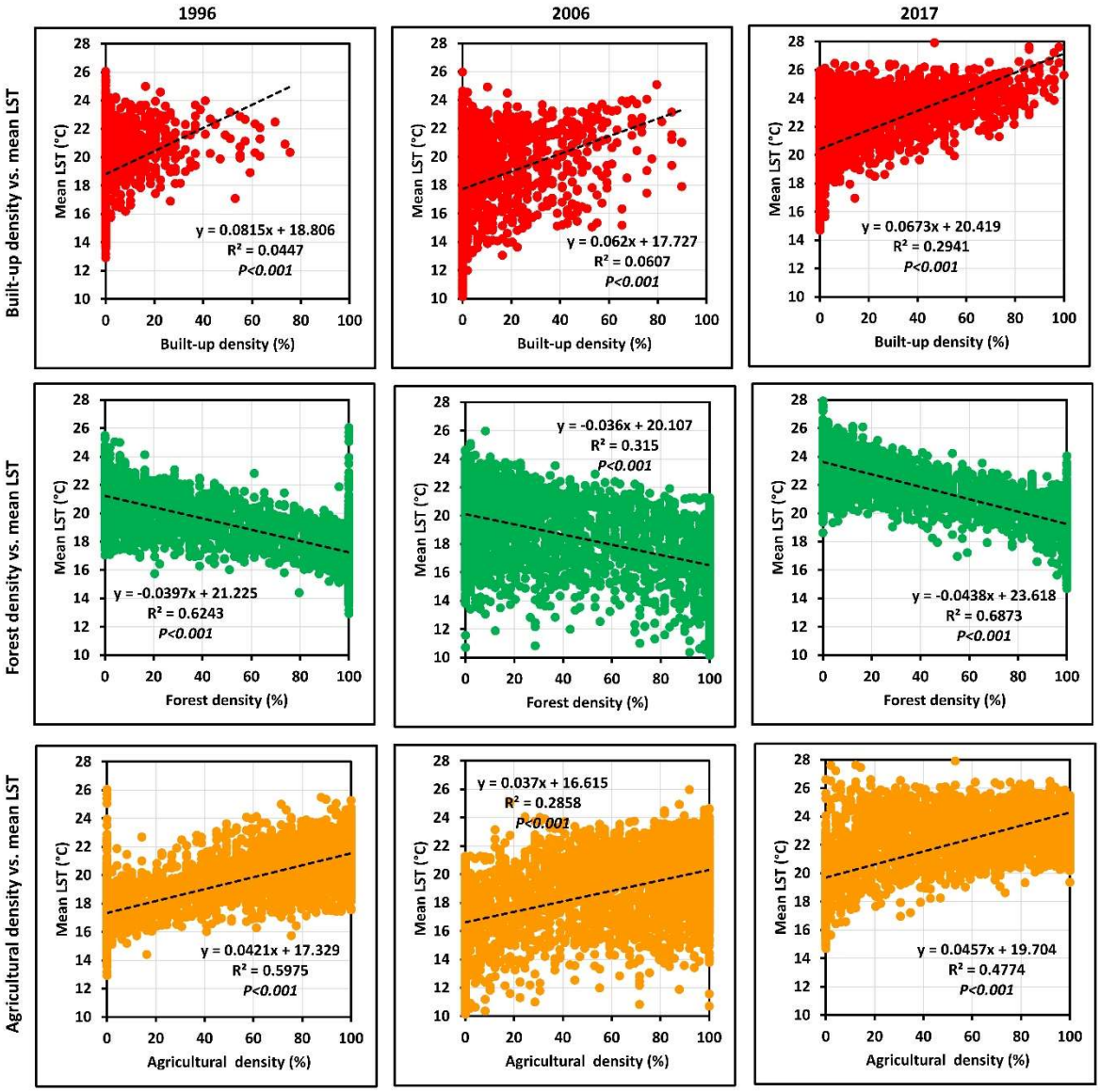

Figure. 9b. Scatterplots showing the relationship between the densities of BL, FL, AL, and mean LST

4. Discussion

In this study, we examined the landscape changes and their impacts on LST in Nuwara Eliya, Sri Lanka during the last 21 years (1996 to 2017). The results revealed that the urbanization pattern of Nuwara Eliya was concentrated around the city center areas in 1996 which then expanded towards the southern, southwestern, northwestern, and eastern parts by 2017. The development pattern of Nuwara Eliya is similar to that of other mountain cities (Kandy) in Sri Lanka [12]. The Built-up land expanded rapidly in the past 21 years (Tables 1 and 2, and Figure 4), with an overall increase of 1,790.6 ha and an annual increase of 85.3 ha. The tourism industry has been reported to be the main driving force of the observed rapid development in the study area as thousands of local and foreign tourists have been visiting Nuwara Eliya [47]. In terms of infrastructural development, the road network improved after the civil war in 2009 and post-war policies attracted significant amounts of foreign capital to Sri Lanka for development projects [62]. The improvement of transportation facilities has reduced travel times resulting in an increase in the numbers of visiting tourists. The number visiting tourists had a 10.1% growth rate from 2000 to 2017 [63,64], and the number of visitors staying overnight increased from 122,334 to 642,162 from 2000 to 2017[63]. The accelerated urbanization rates in the study area can be attributed to the increasing population (583,716 in 1981, 702,689 in 2001, and 711,644 in 2012 [65]) and the increase in the number of tourists visiting Nuwara Eliya. Other

studies in mountain cities such as Baguio in the Philippines [13,44], Kandy in Sri Lanka [12][49], Bengaluru in India [66], Bogor in Indonesia [44], and Dalat in Vietnam [44], revealed that green spaces, such as forests, declined due to urban development pressure in their respective study areas. However, out study revealed that the forest areas were intact throughout the study period owing to strong governmental policies on forest preservation. Most of the forest areas located in Nuwara Eliya are protected. This has resulted in other LULC types other than forests being consumed. Our results demonstrate that BL expanded mainly at the expense of agricultural areas (Figure 5a).

The highest mean LST values were recorded around the city center (URZ_1) in all the three time points and the fraction of BL increased by 32.4%, 48.7%, and 58.7%, while the fraction of AL decreased by 43.6%, 29.6%, and 15.8% in 1996, 2006, and 2017, respectively. The mean LST had a significant positive relationship with the fraction of BL in all the three time-points. The results revealed that the fraction of BL greatly influenced the LSTI in Nuwara Eliya. During the last 21 years (1996, the mean LST of the city center zone (URZ_1) increased by 4.7 °C due to rapid urban expansion. At the same time, the fraction of the BL increased by 26.3% in URZ_1. Conversely, the mean LST had a strong and significant negative relationship with the fraction of FL ($p<0.001$). This result is similar to the pattern observed in other mountain cities in Asia [12,13].

The relationship between the mean LST and the fraction of AL was different in all the three time-points. The mean LST showed a significantly strong positive relationship with the fraction of AL in 1996 while in 2006, the relationship was significantly weak positive. However, in 2017, the relationship became weak negative. We observed that poorly managed agricultural lands were converted into built-up land during the past 21 years. The average fraction of AL exhibited a decreasing pattern, with values of 38.7%, 35.8%, and 27.2% in 1996, 2006, and 2017, respectively. This result is similar to the fact observed for the other mountain cities in Sri Lanka [12]. This pattern is critical evidence for policymakers to introduce a proper mechanism for minimizing the adverse impacts associated with the rapid changes in the urbanization of the study area. The observed urban development impact on agricultural land could negatively affect the production of unique upcountry agricultural products such as exotic vegetables, fruits, cut flowers, and world-famous Ceylon tea. Further, unplanned development could cause several environmental issues [57], such as increasing soil erosion [67], and landslides [68][69][70]. The rapid development of built-up land resulting in increased levels of LST could negatively affect the tourism industry. Policies should be implemented to maintain the natural beauty of Nuwara Eliya for the sustainable tourism industry. Most tourists wish to enjoy the landscape and comfortable climate of the area [47][57].

The change in the urban-rural pattern provides a clear picture of urbanization pattern in the study area. The urban-rural zones were demarcated using the fraction of BL (<10%). The rural zone exhibited a shifting pattern from 1996 to 2017. The rural zone located in URZ_5 (1 km from the city center) in 1996 and the rural zone located in URZ_6 (1.2 km from the city center) in 2006, had shifted to URZ_{18} by 2017 (3.8 km from the city center) (Figure 6a). Rapid changes to built-up land resulted in a shift in the rural zone away from the city center. The result shows that the temperature of URZ_1 was higher than that of the rural zone margin, with values of 1.0, 1.3, and 3.5 °C in 1996, 2006, and 2017, respectively. Previous research has shown a similar trend in the shifting rural zone [12,13]. The Δ mean LST had a strong positive relationship with the Δ fraction of BL and a strong negative relationship with the Δ fraction FL. However, the relationship between the Δ mean LST and Δ fraction of AL shifted from positive (1996 and 2006) to negative (2017). Policymakers should pay much attention to the shifting of the urban zone.

The mixture of land use types which is important for controlling LST [71] was investigated based on two indices i.e., the AL/FL and BL/FL fraction ratios. The results showed that the AL/FL fraction ratio decreased from 1996 to 2017 (Figure 7a). The maximum AL/FL fraction ratio declined with values of 3.3, 2.3, and 1.3 in 1996, 2006, and 2017, respectively. The mean LST exhibited a significantly strong positive relationship with the AL/FL fraction ratio in 1996 and 2006. However, the degree of the relationship became weaker in 2017 due to the changes in the AL of the study area. The Δ mean LST exhibited a positive relationship with the Δ AL/FL fraction ratio over the three time-points (Figure 7c). On the other hand, the result of the BL/FL fraction ratio provided an indicator for

the LSTI pattern in the study area. Changes in built-up land have been proven to be vital in understanding the LST changing pattern in urban areas [19,32,72]. The maximum BL/FL fraction ratio increased with values of 1.7, 2.3, and 3.4 (URZ_1) in 1996, 2006, and 2017, respectively. This resulted in an increase in the mean LST over the 21-year study period (Figure 8a). The increasing BL/FL fraction ratio directly affected the LSTI in the study area as the mean LST had a significantly strong relationship with the BL/FL fraction ratio over the 21-year study period.

The spatial distribution pattern of the BL, FL, and AL densities provided vital information to understand the distribution pattern of the study area. The linear regression analysis results also revealed the vital formation of capturing the land use mixture of the study area. The average density of BL increased with values of 1.3%, 3.5%, and 9.2% while the density of AL decreased with values 37.6%, 35.9%, and 29.2% in 1996, 2006, and 2017, respectively (Figure 9a). This pattern indicates that the BL density has been increasing in the last 21 years. It is based on the linear regression analysis result between mean LST and the density of BL. The coefficient of determination (R^2) between mean LST and the density of BL increased as 0.04 to 0.29 from 1996 to 2017. It shows that the density of BL had a significant influence on the increase of LST in the study area. Same times, the R^2 between mean LST and the density of AL declined as 0.59 to 0. 47 from 1996 to 2017. It shows that AL density has a positive influence on the increase of LST. The only density of FL influenced to control the LST in the study area with the negative strong significant relationship (Figure 9b). Most of the previous studies have combined AL as green spaces, but AL of the Nuwara Eliya area has been positively influencing to the increase of LST in the three time points. The policymakers and planners need to consider maintaining the mixture of land use to control the LST pattern in the future.

All in all, the rapid increase of built-up areas has been the main force driving the recorded high temperatures in 2017 compared to 2006 and 1996. The Δ mean LST exhibited a positive relationship with the Δ BL/FL fraction ratio over the three time-points (Figure 8c). Previous research has demonstrated that having a mixture of land use types results can reduce temperatures in urban areas [71]. Forest coverage will be maintained at a similar level due to governmental policies. However, rapidly developing urban areas require proper urban planning to maintain sustainability. We have noticed: (1) the present urban development pattern is unplanned, and (2) the walls and roofs of most of the buildings are green in color to maintain the greening concept, which is vital for reducing the indoor temperature [73,74]. Sustainable development can be achieved by constructing a green belt along the main road, schools, hospitals, and other government buildings. The present development pattern more forced to horizontal development than vertical development. The vertical development will benefit to keep more land free. Vertical development can be used as a proxy indicator to understand urban-development intensity [75][76]. In addition, tree cover plays a vital role in reducing the impacts of LST in urban areas [77]. We believe that the current urban planning must focus on sustainability to protect this popular tourist destination in Sri Lanka. The findings of this study can be used as an indicator for reorienting current urban planning policies to improve Nuwara Eliya.

5. Conclusions

The spatial distribution of the LST provides vital information for understanding the local climatic variation of the cities and can be used as a proxy indicator to introduce sufficient measures to minimize the negative impacts associated with high LST. This study revealed that Nuwara Eliya has undergone rapid urban development during the past 21 years. In addition, this study used multiple images to extract the median annual LST for 1996, 2006, and 2017. Use of multiple images will provide a better result to understand the LST pattern of the area. The city center temperatures have increased by 4.7 °C. The urban-rural zone have shifted away from the city center resulting in a warmer city center than the rural zone. It shows the rapid development was spreading towards rural zones, especially in 2017. The rapid increase in the BL fraction was affected by the decreasing fraction of AL. Mean LST exhibited a strong positive relationship with the BL/FL fraction ratio, and a decreasing positive relationship with the AL/FL fraction ratio. The density of AL and BL had a positive relationship with mean LST indicating that both BL and AL influenced the increase in the

LST of the study area. on the other hand, the government policies have been protecting the FL resulting in minimal changes during the last 21 years. It has been the main source to control the LST pattern. A mixture of land use types is vitally important to control the LST increasing. The grid-based analysis showed that the relationship between mean LST and density of BL has been increasing due to the increasing trend of BL in the study area. BL has played a vital role to control mean LST of the study area. Policy makers need to consider the importance of the land use mixture to reduce the impacts of high LST in the study area. Nuwara Eliya is renowned as a tourist destination in Sri Lanka. The future urban policy must focus on maintaining the natural splendor of the Nuwara Eliya to promote tourism in the study area and Sri Lanka. The findings of this study can be used as an indicator to introduce sustainable future landscape and urban planning to protect the world-renowned tourist hub of Sri Lanka.

Author Contributions: The corresponding author, M.R., proposed the topic and spearheaded the data processing and analysis, as well as the writing of the manuscript. Y.M., D.M.S.L.B. and M.S. helped in the design, research implementation and analysis and writing of the manuscript.

Funding:

Acknowledgments:

Conflicts of Interest: The authors declare no conflicts of interest.

Appendix A

Table A1. Properties of the Landsat images (Level 2) used in this study.

Sensor	Scene ID	Acquisition Date	Time (GMT)	Cloud cover (%) in Landsat title
Landsat 5 TM	LT05_L1TP_141055_19960221_20170106_01_T1	1996-02-21	03:59:45	19
	LT05_L1TP_141055_19960308_20170106_01_T1	1996-03-08	04:00:49	6
	LT05_L1TP_141055_19960324_20170105_01_T1	1996-03-24	04:01:51	11
	LT05_L1TP_141055_19960409_20170105_01_T1	1996-04-09	04:02:51	46
	LT05_L1TP_141055_19960425_20170104_01_T1	1996-04-25	04:03:49	9
	LT05_L1TP_141055_19960511_20170104_01_T1	1996-05-11	04:04:46	9
	LT05_L1TP_141055_19960527_20170104_01_T1	1996-05-27	04:05:41	29
	LT05_L1TP_141055_19960730_20170103_01_T1	1996-07-30	04:09:06	78
	LT05_L1TP_141055_19960815_20170103_01_T1	1996-08-15	04:09:56	66
	LT05_L1TP_141055_19960831_20170103_01_T1	1996-08-31	04:10:48	41
	LT05_L1TP_141055_19960916_20170102_01_T1	1996-09-16	04:11:41	70
	LT05_L1TP_141055_19961002_20170102_01_T1	1996-10-02	04:12:33	48
	LT05_L1TP_141055_19961103_20170102_01_T1	1996-11-03	04:14:09	38
	LT05_L1TP_141055_19961119_20170101_01_T1	1996-11-19	04:14:53	19
	LT05_L1TP_141055_19961205_20170101_01_T1	1996-12-05	04:15:40	84
Landsat 5 TM	LT05_L1TP_141055_20060131_20161123_01_T1	2006-01-31	04:44:06	46
	LT05_L1TP_141055_20060216_20161123_01_T1	2006-02-16	04:44:28	28
	LT05_L1TP_141055_20060304_20161122_01_T1	2006-03-04	04:44:49	41
	LT05_L1TP_141055_20060405_20161123_01_T1	2006-04-05	04:45:26	10
	LT05_L1TP_141055_20060421_20161122_01_T1	2006-04-21	04:45:41	68
	LT05_L1TP_141055_20060507_20161122_01_T1	2006-05-07	04:45:55	33

Peer-reviewed version available at Sustainability 2019, 11, 5517; doi:10.3390/su11195517

	LT05_L1TP_141055_20060523_20161121_01_T1	2006-05-23	04:46:07	31
	LT05_L1TP_141055_20060608_20161121_01_T1	2006-06-08	04:46:23	27
	LT05_L1TP_141055_20060624_20161121_01_T1	2006-06-24	04:46:39	72
	LT05_L1TP_141055_20060710_20161120_01_T1	2006-07-10	04:46:53	30
	LT05_L1TP_141055_20060811_20161119_01_T1	2006-08-11	04:47:17	79
	LT05_L1TP_141055_20060827_20161119_01_T1	2006-08-27	04:47:29	45
	LT05_L1TP_141055_20060912_20161119_01_T1	2006-09-12	04:47:41	57
	LT05_L1TP_141055_20060928_20161119_01_T1	2006-09-28	04:47:52	55
	LT05_L1TP_141055_20061014_20161118_01_T1	2006-10-14	04:48:03	22
	LT05_L1TP_141055_20061030_20161118_01_T1	2006-10-30	04:48:13	30
	LT05_L1TP_141055_20061115_20161118_01_T1	2006-11-15	04:48:21	60
	LC08_L1TP_141055_20170113_20170311_01_T1	2017-01-13	04:54:05	3
	LC08_L1TP_141055_20170129_20170214_01_T1	2017-01-29	04:53:59	40
	LC08_L1TP_141055_20170214_20170228_01_T1	2017-02-14	04:53:52	68
	LC08_L1TP_141055_20170302_20170316_01_T1	2017-03-02	04:53:46	64
	LC08_L1TP_141055_20170318_20170328_01_T1	2017-03-18	04:53:36	13
	LC08_L1TP_141055_20170403_20170414_01_T1	2017-04-03	04:53:29	16
	LC08_L1TP_141055_20170419_20170501_01_T1	2017-04-19	04:53:20	15
	LC08_L1TP_141055_20170505_20170515_01_T1	2017-05-05	04:53:13	32
	LC08_L1TP_141055_20170606_20170616_01_T1	2017-06-06	04:53:34	54
Landsat 8	LC08_L1TP_141055_20170622_20170630_01_T1	2017-06-22	04:53:40	28
OLI/TIRS	LC08_L1TP_141055_20170708_20170716_01_T1	2017-07-08	04:53:43	44
	LC08_L1TP_141055_20170724_20170809_01_T1	2017-07-24	04:53:49	38
	LC08_L1TP_141055_20170809_20170824_01_T1	2017-08-09	04:53:56	47
	LC08_L1TP_141055_20170825_20170913_01_T1	2017-08-25	04:54:00	38
	LC08_L1TP_141055_20170910_20170927_01_T1	2017-09-10	04:54:02	61
	LC08_L1TP_141055_20170926_20171013_01_T1	2017-09-26	04:54:07	82
	LC08_L1TP_141055_20171012_20171024_01_T1	2017-10-12	04:54:12	76
	LC08_L1TP_141055_20171028_20171108_01_T1	2017-10-28	04:54:13	19
	LC08_L1TP_141055_20171113_20171121_01_T1	2017-11-13	04:54:10	38
	LC08_L1TP_141055_20171215_20171223_01_T1	2017-12-15	04:54:05	32

A2. The code used to generate median temperature of Landsat 5 TM images for 1996 and 2006.

```
// Export Landsat 5 SR data
/**
 * Function to mask clouds based on the pixel_qa band of Landsat SR data.
 * @param {ee.Image} image Input Landsat SR image
 * @return {ee.Image} Cloudmasked Landsat image
 */
var cloudMaskL457 = function(image) {
  var qa = image.select('pixel_qa');
  // If the cloud bit (5) is set and the cloud confidence (7) is high
```

Peer-reviewed version available at Sustainability 2019, 11, 5517; doi:10.3390/su11195517


```
    // or the cloud shadow bit is set (3), then it's a bad pixel.
    var cloud = qa.bitwiseAnd(1 << 5)
                    .and(qa.bitwiseAnd(1 << 7))
                    .or(qa.bitwiseAnd(1 << 3));
    // Remove edge pixels that don't occur in all bands
    var mask2 = image.mask().reduce(ee.Reducer.min());
    return image.updateMask(cloud.not()).updateMask(mask2);
};
//Load the Landsat 5 data collection - example for B6
{
var col = ee.ImageCollection('LANDSAT/LT05/C01/T1_SR')
.map(cloudMaskL457)
.filterDate('1996-01-01','1996-12-30')
.select( ['B6'])
.filterBounds(geometry);
}
//Compute the median of the collection -example for B6
{
var image = col.median().clip(geometry);
print(image, 'Selected band');
Map.addLayer(image);
}
// Export the B6, specifying scale and region.
Export.image.toDrive({
    image: image,
    description: 'B6',
    scale: 30,
    region: geometry,
    maxPixels:1e13,
    folder: 'Landsat 5 data collection',
    skipEmptyTiles: true
});
// Export the B6 information as table.
Export.table.toDrive({
    collection: col,
    description: 'B6_information',
    fileFormat: 'CSV',
    folder:'Landsat 5 data collection'
});
```

```
// Get the number of collections.
var count = col.size();
print('Count: ', count);
// Get the date range of images in the collection.
var range = col.reduceColumns(ee.Reducer.minMax(), ["system:time_start"])
print('Date range: ', ee.Date(range.get('min')), ee.Date(range.get('max')))
```

A3. The code used to generate median temperature of Landsat 8 images for 2017.

```
// Export Landsat 8 SR data
/**
 * Function to mask clouds based on the pixel_qa band of Landsat 8 SR data.
 * @param {ee.Image} image input Landsat 8 SR image
 * @return {ee.Image} cloudmasked Landsat 8 image
 */
function maskL8sr(image) {
  // Bits 3 and 5 are cloud shadow and cloud, respectively.
  var cloudShadowBitMask = (1 << 3);
  var cloudsBitMask = (1 << 5);
  // Get the pixel QA band.
  var qa = image.select('pixel_qa');
  // Both flags should be set to zero, indicating clear conditions.
  var mask = qa.bitwiseAnd(cloudShadowBitMask).eq(0)
                 .and(qa.bitwiseAnd(cloudsBitMask).eq(0));
  return image.updateMask(mask);
}
//Load the Landsat 8 data collection - example for B10
{
var col = ee.ImageCollection('LANDSAT/LC08/C01/T1_SR')
.map(maskL8sr)
.filterDate('2018-01-01','2018-12-30')
.select(['B10'])
.filterBounds(geometry);
}
//Compute the median of the collection - example for B10
{
var image = col.median().clip(geometry);
print(image, 'Selected band');
Map.addLayer(image);
}
```

Peer-reviewed version available at Sustainability 2019, 11, 5517; doi:10.3390/su11195517


```
// Export the B10, specifying scale and region.
Export.image.toDrive({
  image: image,
  description: 'B10',
  scale: 30,
  region: geometry,
  maxPixels:1e13,
  folder: 'Landsat 8 data collection',
  skipEmptyTiles: true
});
// Export the B10 information as table.
Export.table.toDrive({
  collection: col,
  description: 'B10_information',
  fileFormat: 'CSV',
  folder:'Landsat 8 data collection'
});
// Get the number of collections.
var count = col.size();
print('Count: ', count);
// Get the date range of images in the collection.
var range = col.reduceColumns(ee.Reducer.minMax(), ["system:time_start"])
print('Date range: ', ee.Date(range.get('min')), ee.Date(range.get('max')))
```

Table A4. Error matrix for the classified 1996 land use/cover map, classified

Classified Data	Reference Data					Total	User's Accuracy (%)
	Built-up	Forest	Agricultural land	Other	Water		
Built-up	72	8	6	3	0	89	80.9
Forest	2	165	10	3	3	183	90.2
Agricultural land	5	17	140	2	2	166	84.3
Other land	2	2	3	34	1	42	81.0
Water	0	2	2	0	16	20	80.0
Total	81	194	161	42	22	500	
Producer's accuracy (%)	88.9	85.1	87.0	81.0	72.7		

Overall Accuracy (%) = 85 %

608 **Table A5.** Error matrix for the classified 2006 land use/cover map, classified

Classified Data	Reference Data					Total	User's Accuracy (%)
	Built-up	Forest	Agricultural land	Other	Water		
Built-up	98	2	5	0	0	105	93.3
Forest	3	182	8	0	0	193	94.3
Agricultural land	4	5	155	1	1	166	93.4
Other land	0	0	1	5	1	7	71.4
Water	0	1	1	1	26	29	89.7
Total	105	190	170	7	28	500	
Producer's accuracy (%)	93.3	95.8	91.2	71.4	92.9		

609 Overall Accuracy (%) = 93 %

610 **Table A6.** Error matrix for the classified 1996 land use/cover map, classified

Classified Data	Reference Data					Total	User's Accuracy (%)
	Built-up	Forest	Agricultural land	Other	Water		
Built-up	110	3	3	1	0	117	94.0
Forest	5	160	7	1	0	173	92.5
Agricultural land	3	2	135	2	1	143	94.4
Other land	2	3	2	33	1	41	80.5
Water	0	1	1	0	24	26	92.3
Total	120	169	148	37	26	500	
Producer's accuracy (%)	91.7	94.7	91.2	89.2	92.3		

611 Overall Accuracy (%) = 92 %

612 ## References

613 1. Chen, X.; Zhang, Y. Impacts of urban surface characteristics on spatiotemporal pattern of land surface
614 temperature in Kunming of China. *Sustain. Cities Soc.* **2017**, *32*, 87–99.
615 2. Thi Van, T.; Xuan Bao, H.D. Study of the impact of urban development on surface temperature using
616 remote sensing in Ho Chi Minh City, Northern Vietnam. *Geogr. Res.* **2010**, *48*, 86–96.
617 3. Ranagalage, M.; Estoque, R.C.; Murayama, Y. An urban heat island study of the Colombo Metropolitan
618 Area, Sri Lanka, based on Landsat data (1997–2017). *ISPRS Int. J. Geo-Information* **2017**, *6*, 189.
619 4. Ranagalage, M.; Estoque, R.C.; Zhang, X.; Murayama, Y. Spatial changes of urban heat island formation
620 in the Colombo District, Sri Lanka: Implications for sustainability planning. *Sustainability* **2018**, *10*.
621 5. Son, N.-T.; Chen, C.-F.; Chen, C.-R.; Thanh, B.-X.; Vuong, T.-H. Assessment of urbanization and urban
622 heat islands in Ho Chi Minh City, Vietnam using Landsat data. *Sustain. Cities Soc.* **2017**, *30*, 150–161.
623 6. Hou, H.; Wang, R.; Murayama, Y. Scenario-based modelling for urban sustainability focusing on
624 changes in cropland under rapid urbanization : A case study of Hangzhou from 1990 to 2035. *Sci. Total*
625 *Environ.* **2019**, *661*, 422–431.
626 7. Alphan, H. Land-use change and urbanization of Adana, Turkey. *L. Degrad. Dev.* **2003**, *14*, 575–586.
627 8. Shalaby, A.; Ghar, M.A.; Tateishi, R. Desertification impact assessment in Egypt using low resolution
628 satellite data and GIS. *Int. J. Environ. Stud.* **2004**, *61*, 375–383.
629 9. El Araby, M. Urban growth and environmental degradation. *Cities* **2002**, *19*, 389–400.

10. Debela, T.H.; Beyene, A.; Tesfahun, E.; Getaneh, A.; Gize, A.; Mekonnen, Z. Fecal contamination of soil and water in sub-Saharan Africa cities: The case of Addis Ababa, Ethiopia. *Ecohydrol. Hydrobiol.* **2018**, *18*, 225–230.
11. Knudsen, A.B.; Slooff, R. Vector-borne disease problems in rapid urbanization: new approaches to vector control. *Bull. World Health Organ.* **1992**, *70*, 1–6.
12. Ranagalage, M.; Dissanayake, D.; Murayama, Y.; Zhang, X.; Estoque, R.C.; Perera, E.; Morimoto, T. Quantifying surface urban heat island formation in the world heritage tropical mountain city of Sri Lanka. *ISPRS Int. J. Geo-Information* **2018**, *7*, 341.
13. Estoque, R.C.; Murayama, Y. Monitoring surface urban heat island formation in a tropical mountain city using Landsat data (1987–2015). *ISPRS J. Photogramm. Remote Sens.* **2017**, *133*, 18–29.
14. Voogt, J.A.; Oke, T.R. Thermal remote sensing of urban climates. *Remote Sens. Environ.* **2003**, *86*, 370–384.
15. Estoque, R.C.; Murayama, Y.; Myint, S.W. Effects of landscape composition and pattern on land surface temperature: An urban heat island study in the megacities of Southeast Asia. *Sci. Total Environ.* **2017**, *577*, 349–359.
16. Weng, Q. A remote sensing – GIS evaluation of urban expansion and its impact on surface temperature in the Zhujiang Delta , China. *Int. J. Remote Sens.* **2014**, *22*, 1999–2014.
17. Singh, P.; Kikon, N.; Verma, P. Impact of land use change and urbanization on urban heat island in Lucknow city, Central India. A remote sensing based estimate. *Sustain. Cities Soc.* **2017**, *32*, 100–114.
18. Mirzaei, P.A. Recent challenges in modeling of urban heat island. *Sustain. Cities Soc.* **2015**, *19*, 200–206.
19. Rousta, I.; Sarif, M.O.; Gupta, R.D.; Olafsson, H.; Ranagalage, M.; Murayama, Y.; Zhang, H.; Mushore, T.D. Spatiotemporal analysis of land use / land cover and its effects on surface urban heat island using Landsat data : A case study of metropolitan city Tehran (1988–2018). *Sustainability* **2018**, *10*, 4433.
20. Oba, G. Urban Heat Island Effect of Addis Ababa City: Implications of Urban Green Spaces for Climate Change Adaptation. *Clim. Chang. Adapt. Africa* **2014**.
21. Tran, H.; Uchihama, D.; Ochi, S.; Yasuoka, Y. Assessment with satellite data of the urban heat island effects in Asian mega cities. *Int. J. Appl. Earth Obs. Geoinf.* **2006**, *8*, 34–48.
22. Van Nguyen, O.; Kawamura, K.; Trong, D.P.; Gong, Z.; Suwandana, E. Temporal change and its spatial variety on land surface temperature and land use changes in the Red River Delta, Vietnam, using MODIS time-series imagery. *Environ. Monit. Assess.* **2015**, *187*.
23. Ayanlade, A. Seasonality in the daytime and night-time intensity of land surface temperature in a tropical city area. *Sci. Total Environ.* **2016**, *557–558*, 415–424.
24. Zhou, D.; Zhang, L.; Hao, L.; Sun, G.; Liu, Y.; Zhu, C. Spatiotemporal trends of urban heat island effect along the urban development intensity gradient in China. *Sci. Total Environ.* **2016**, *544*, 617–626.
25. Marconcini, M.; Metz, A.; Esch, T.; Zeidler, J. Global urban growth monitoring by means of SAR data. *Int. Geosci. Remote Sens. Symp.* 2014, 1477–1480.
26. Paranunzio, R.; Ceola, S.; Laio, F.; Montanari, A. Evaluating the effects of urbanization evolution on air temperature trends using nightlight satellite data. *Atmosphere (Basel).* **2019**, *10*, 117.
27. Zhou, Y.; Smith, S.J.; Zhao, K.; Imhoff, M.; Thomson, A.; Bond-Lamberty, B.; Asrar, G.R.; Zhang, X.; He, C.; Elvidge, C.D. A global map of urban extent from nightlights. *Environ. Res. Lett.* **2015**, *10*, 2000–2010.
28. Weng, Q. Thermal infrared remote sensing for urban climate and environmental studies: Methods, applications, and trends. *ISPRS J. Photogramm. Remote Sens.* **2009**, *64*, 335–344.
29. Weng, Q.; Lu, D.; Schubring, J. Estimation of land surface temperature-vegetation abundance relationship for urban heat island studies. *Remote Sens. Environ.* **2004**, *89*, 467–483.

673 30. Bhaduri, B.; Bright, E.; Coleman, P.; Urban, M.L. LandScan USA: A high-resolution geospatial and
674 temporal modeling approach for population distribution and dynamics. *GeoJournal* **2007**, *69*, 103–117.
675 31. Zhang, X.; Estoque, R.C.; Murayama, Y. An urban heat island study in Nanchang City, China based on
676 land surface temperature and social-ecological variables. *Sustain. Cities Soc.* **2017**, *32*, 557–568.
677 32. Dissanayake, D.; Morimoto, T.; Ranagalage, M.; Murayama, Y. Impact of Urban Surface Characteristics
678 and Socio-Economic Variables on the Spatial Variation of Land Surface Temperature in Lagos City ,
679 Nigeria. *Sustainability* **2019**, *11*, 1–23.
680 33. Bhargava, A., S. Lakmini, and S. Bhargava. Urban Heat Island Effect: It's Relevance in Urban Planning.
681 *J. Biodivers. Endanger. Species* **2017**, *05*, 1–4.
682 34. Xu, S. An approach to analyzing the intensity of the daytime surface urban heat island effect at a local
683 scale. *Environ. Monit. Assess.* **2009**, *151*, 289–300.
684 35. Li, Y.Y.; Zhang, H.; Kainz, W. Monitoring patterns of urban heat islands of the fast-growing Shanghai
685 metropolis, China: Using time-series of Landsat TM/ETM+ data. *Int. J. Appl. Earth Obs. Geoinf.* **2012**, *19*,
686 127–138.
687 36. Senanayake, I.P.; Welivitiya, W.D.D.P.; Nadeeka, P.M. Remote sensing based analysis of urban heat
688 islands with vegetation cover in Colombo city, Sri Lanka using Landsat-7 ETM+ data. *Urban Clim.* **2013**,
689 *5*, 19–35.
690 37. Sakakibara, Y.; Owa, K. Urban-rural temperature differences in coastal cities: Influence of rural sites. *Int.*
691 *J. Climatol.* **2005**, *25*, 811–820.
692 38. Myint, S.W.; Brazel, A.; Okin, G.; Buyantuyev, A. Combined effects of impervious surface and vegetation
693 Cover on air temperature variations in a rapidly expanding desert city. *GIScience Remote Sens.* **2010**, *47*,
694 301–320.
695 39. Ravanelli, R.; Nascetti, A.; Cirigliano, R.V.; Di Rico, C.; Leuzzi, G.; Monti, P.; Crespi, M. Monitoring the
696 impact of land cover change on surface urban heat island through Google Earth Engine: Proposal of a
697 global methodology, first applications and problems. *Remote Sens.* **2018**, *10*, 1–21.
698 40. Parastatidis, D.; Mitraka, Z.; Chrysoulakis, N.; Abrams, M. Online global land surface temperature
699 estimation from landsat. *Remote Sens.* **2017**, *9*, 1–17.
700 41. Stewart, I.; Oke, T. Classifying urban climate field sites by "local climate zones": the case of nagano ,
701 japan. *seventh Int. Conf. Urban Clim.* **2009**, 1–5.
702 42. Oke, T.R. *Initial Guidance to Obtain Representative Meteorological Observations at Urban Sites*; 2004;
703 43. Ranagalage, M.; Estoque, R.C.; Handayani, H.H.; Zhang, X.; Morimoto, T.; Tadono, T.; Murayama, Y.
704 Relation between urban volume and land surface temperature : A comparative study of planned and
705 traditional cities in Japan. *Sustainability* **2018**, *10*, 1–17.
706 44. Estoque, R.C.; Murayama, Y. Quantifying landscape pattern and ecosystem service value changes in
707 four rapidly urbanizing hill stations of Southeast Asia. *Landsc. Ecol.* **2016**, *31*, 1481–1507.
708 45. Estoque, R.C.; Murayama, Y. City Profile: Baguio. *Cities* **2013**, *30*, 240–251.
709 46. Crossette, B. *The Great Hill Stations of Asia*; New York, 1999; Vol. 73;.
710 47. Jayasinghe, M.K.D.; Gnanapala, W.K.A..; Sandaruwani, J.A.R.. Factors affecting tourists' perception and
711 satisfaction in Nuwara Eliya, Sri Lanka. *Ilorin J. Econ. Policy* **2015**, *2*, 1–15.
712 48. Weerasinghe, W.W.K. Transformation of the landscape of Nuwara-Eliya. Ph.D. Thesis, University of
713 Moratuwa, Colombo, Sri Lanka, 2003.
714 49. Dissanayake, D.; Morimoto, T.; Ranagalage, M.; Murayama, Y. Land-Use/Land-Cover Changes and
715 Their Impact on Surface Urban Heat Islands: Case Study of Kandy City, Sri Lanka. *Climate* **2019**, *7*, 99.

50. Google Erath Engine, Landsat collection structure. Available online: https://developers.google.com/earth-engine/landsat (accessed on 25 May 2019)
51. Google Erath Engine, Image collection reductions Available online: https://developers.google.com/earth-engine/reducers_image_collection (accessed on 25 May 2019)
52. Sobrino, J.A.; Jiménez-Muñoz, J.C.; Paolini, L. Land surface temperature retrieval from LANDSAT TM 5. *Remote Sens. Environ.* **2004**, *90*, 434–440.
53. Zhang, Y.; Odeh, I.O.A.; Han, C. Bi-temporal characterization of land surface temperature in relation to impervious surface area, NDVI and NDBI, using a sub-pixel image analysis. *Int. J. Appl. Earth Obs. Geoinf.* **2009**, *11*, 256–264.
54. Huang, C.; Davis, L.S.; Townshend, J.R.G. An assessment of support vector machines for land cover classification. *Int. J. Remote Sens.* **2002**, *23*, 725–749.
55. Xiaojun Yang Parameterizing Support Vector Machines for Land Cover Classification. *Photogramm. Eng. Remote Sensing* **2011**, *77*.
56. Shi, D.; Yang, X. Support Vector Machines for Land Cover Mapping from Remote Sensor Imagery. In *Monitoring and Modeling of Global Changes: A Geomatics Perspective*; Springer, Dordrecht., 2015; pp. 265–279 ISBN 978-94-017-9812-9.
57. Ranagalage, M.; Wang, R.; Gunarathna, M.H.J.P.; Dissanayake, D.; Murayama, Y.; Simwanda, M. Spatial forecasting of the landscape in rapidly urbanizing hill stations of South Asia : A case study of Nuwara Eliya, Sri Lanka (1996–2037). *Remote Sens.* **2019**, *11*, 1743.
58. Gunaalan, K.; Ranagalage, M.; Gunarathna, M.H.J.P.; Kumari, M.K.N.; Vithanage, M.; Srivaratharasan, T.; Saravanan, S.; Warnasuriya, T.W.S. Application of geospatial techniques for groundwater quality and availability assessment: A case study in Jaffna Peninsula, Sri Lanka. *ISPRS Int. J. Geo-Information* **2018**, *7*.
59. Simwanda, M.;Ranagalage, M.; Estoque, R.C.; Murayama, Y. Spatial analysis of surface urban heat islands in four rapidly growing African cities. *Remote Sens.* **2019**, *11*, 1–20.
60. Dissanayake, D.; Morimoto, T.; Murayama, Y.; Ranagalage, M. Impact of Landscape Structure on the Variation of Land Surface Temperature in Sub-Saharan Region: A Case Study of Addis Ababa using Landsat Data (1986–2016). *Sustainability* **2019**, *11*, 2257.
61. Lanka, D. forest of S. *Forest Ordinance*; 1908;
62. Subasinghe, S.; Estoque, R.C.; Murayama, Y. Spatiotemporal analysis of urban growth using GIS and remote sensing : A Case Study of the Colombo Metropolitan Area , Sri Lanka. *Int. J. Geo-Information* **2016**, *5*, 1–19.
63. Sri Lanka Tourism Development Authority , *Annual Statistical Report 2000*; 2000; Available online: https://www.scribd.com/fullscreen/36055292?access_key=key-18nb580f7hrixixeltt8 (accessed on 25 July 2019).
64. Sri Lanka Tourism Development Authority , *Annual Statistical Report 2017*; 2017; Available online: http://www.sltda.lk/sites/default/files/annual-statical-report-2017.pdf (accessed on 25 July 2019).
65. Census of Population and Housing 2012. Available online: http://www.statistics.gov.lk/pophousat/cph2011/index.php?fileName=Activities/TentativelistofPublica tio ns (accessed on 27 June 2019).
66. Sultana, S.; Satyanarayana, A.N.V. Urban heat island intensity during winter over metropolitan cities of India using remote-sensing techniques: impact of urbanization. *Int. J. Remote Sens.* **2018**, *39*, 6692–6730.
67. Dissanayake, D.; Morimoto, T.; Ranagalage, M. Accessing the soil erosion rate based on RUSLE model for sustainable land use management : a case study of the Kotmale watershed , Sri Lanka. *Model. Earth*

Syst. Environ. **2018**, *4*, 1–16.

68. Ranagalage, M. Landslide hazards assessment in Nuwara Eliya district in Sri Lanka. In Proceedings of the Japanese Geographical meeting; 2017; p. 100336.
69. Perera, E.N.C.; Jayawardana, D.T.; Jayasinghe, P.; Ranagalage, M. Landslide vulnerability assessment based on entropy method: a case study from Kegalle district, Sri Lanka. *Model. Earth Syst. Environ.* **2019**.
70. Perera, E.N.C.; Jayawardana, D.T.; Ranagalage, M.; Jayasinghe, P. Spatial multi criteria evaluation (SMCE) model for landslide hazard zonation in tropical hilly environment: A case study from Kegalle. *Geoinform. Geostat. Overv.* **2018**, *S3*,
71. Thanh Hoan, N.; Liou, Y.-A.; Nguyen, K.-A.; Sharma, R.; Tran, D.-P.; Liou, C.-L.; Cham, D. Assessing the effects of land-use types in surface urban heat islands for developing comfortable living in Hanoi City. *Remote Sens.* **2018**, *10*, 1965.
72. Yuan, F.; Bauer, M.E. Comparison of impervious surface area and normalized difference vegetation index as indicators of surface urban heat island effects in Landsat imagery. *Remote Sens. Environ.* **2007**, *106*, 375–386.
73. Galagoda, R.U.; Jayasinghe, G.Y.; Halwatura, R.U.; Rupasinghe, H.T. The impact of urban green infrastructure as a sustainable approach towards tropical micro-climatic changes and human thermal comfort. *Urban For. Urban Green.* **2018**, *34*, 1–9.
74. Manawadu, L. Ranagalage, M. Urban heat islands and vegetation cover as a controlling factor. In Proceedings of the Proceedings of the International Forestry and Environment Symposium 2013 of the Department of Forestry and Environmental Science, University of Sri Jayewardenepura, Sri Lanka.; 2013; p. 125.
75. Estoque, R. C., Murayama, Y., Ranagalage, M., Hou, H., Subasinghe, S., Gong, H., ... & Zhang, X.. Validating ALOS PRISM DSM-derived surface feature height : Implications for urban volume estimation. *Tsukuba Geoenvironmental Sci.* **2017**, *13*, 13–22.
76. Ranagalage, M. Murayama, Y. Measurement of urban built-up volume using remote sensing data and geospatial techniques. *Tsukuba Geoenvironmental Sci.* **2018**, *14*, 19–29.
77. Handayani, H.H.; Murayama, Y.; Ranagalage, M.; Liu, F.; Dissanayake, D. Geospatial analysis of horizontal and vertical urban expansion using multi-spatial resolution data : A case study of Surabaya , Indonesia. *Remote Sens.* **2018**, *10*, 25.